photonics

MDPI

Letter

Operation of a Single-Frequency Bismuth-Doped Fiber Power Amplifier near 1.65 µm

Grzegorz Gomółka [1], Monika Krajewska [1], Małgorzata Kaleta [1], Aleksandr M. Khegai [2], Sergey V. Alyshev [2], Aleksey S. Lobanov [3], Sergei V. Firstov [2] and Michał Nikodem [1,*]

1 Department of Optics and Photonics, Wroclaw University of Science and Technology, Wybrzeze Wyspianskiego 27, 50-370 Wroclaw, Poland; grzegorz.gomolka@pwr.edu.pl (G.G.); 236704@student.pwr.edu.pl (M.K.); 245004@student.pwr.edu.pl (M.K.)

2 Prokhorov General Physics Institute of the Russian Academy of Sciences, Dianov Fiber Optics Research Center, 38 Vavilov str., 119333 Moscow, Russia; khegai@fo.gpi.ru (A.M.K.); alyshs@fo.gpi.ru (S.V.A.); fir@fo.gpi.ru (S.V.F.)

3 Institute of Chemistry of High Purity Substances, Russian Academy of Sciences, 29 Tropinin str., 603600 Nizhny Novgorod, Russia; lobanov@ihps.nnov.ru

* Correspondence: michal.nikodem@pwr.edu.pl

Received: 6 November 2020; Accepted: 8 December 2020; Published: 9 December 2020

Abstract: The spectral range between 1650 and 1700 nm is an interesting region due to its potential applications in optical telecommunication and optical-based methane sensing. Unfortunately, the availability of compact and simple optical amplifiers with output powers exceeding tens of milliwatts in this spectral region is still limited. In this paper, a single-frequency continuous-wave bismuth-doped fiber amplifier (BDFA) operating at 1651 and 1687 nm is presented. With the improved signal/pump coupling and modified pump source design, the output powers of 163 mW (at 1651 nm) and 197 mW (at 1687 nm) were obtained. Application of the BDFA to the optical spectroscopy of methane near 1651 nm is also described. We demonstrate that the BDFA can be effectively used for signal amplitude enhancement in photothermal interferometry.

Keywords: optical amplifiers; doped fiber amplifiers; near-infrared; molecular gas spectroscopy; photothermal spectroscopy; heterodyne detection

1. Introduction

Over the last few decades, fiber-based optical amplifiers have proven to be effective power amplifiers with a number of advantages, such as high gain, a high output power, a low noise figure, polarization independence, and broad amplification spectral bands. Fiber-based amplifiers are capable of providing gain in numerous spectral regions, from the visible light to near-infrared region. However, in some spectral regions, the availability of proper gain medium, fiber chemical composition, and manufacturing issues are still critical problems. One of the research gaps is the spectral range beyond 1650 nm, which can potentially be used not only to extend existing telecommunication windows, but also in applications such as laser eye surgery [1,2] and the chemical sensing of hydrocarbons such as methane [3–5] and ethane [6]. Thulium-doped fiber amplifiers (TDFAs) can be used in this spectral region. However, because these wavelengths are at the edge of the thulium gain band, the highest demonstrated saturation power near 1650 nm was less than 50 mW [7,8]. Raman amplifiers are capable of providing much higher output powers, but require long (about 1 km or more) pieces of specialty fiber [9] and very high (watt level) pumping powers [10]. In this respect, bismuth-doped fiber amplifiers are interesting alternatives that may be used to obtain decent output powers (beyond 100 mW) in a simple and compact configuration, similar to rare earth-doped amplifiers.

Bismuth-doped fibers (BDFs) are an interesting group of active fibers that are capable of covering spectral regions unavailable for rare-earth-doped fibers [11]. As Bi-doped fibers have luminescence properties dependent on the host glass, they are a quite flexible medium for photonic system development [12]. For example, broadband emission covering a range from 1150 up to 1500 nm has been demonstrated using Bi-doped aluminosilicate and phosphosilicate glass fibers [13–16], while Bi-doped germanosilicate fibers can also be used as gain media beyond 1600 nm [17–20].

This paper presents a continuation of our earlier experiments, in which the performance of a bismuth-doped fiber amplifier (BDFA) at 1651 [21] and 1687 nm [22] was analyzed. Previously, the output powers of ~87 and ~107 mW were obtained at 1651 and 1687 nm, respectively. These results were limited by two issues. The first was stimulated Brillouin scattering (SBS) in BDF, which turned out to affect the BDFA gain when high pumping powers were used [21]. The other issue was the efficiency of coupling the signal (at 1651 or 1687 nm) and the pump (at 1550 nm). In this paper, a modified configuration of the amplifier is demonstrated. Improved signal/pump coupling and a new pump source enabled output powers of 163 mW (at 1651 nm) and 197 mW (at 1687 nm) to be obtained, which are almost twice as high as those achieved with the previous amplifier design.

The paper is organized as follows. The second section describes the experimental setup. We present a new pump source (Section 2.1) and demonstrate its impact on the reduction of backscattered light due to SBS (Section 3.1). The performance of the BDFA (including the output power dependence on the pump power and the input power at two wavelengths) is presented in Section 3.2. In Section 3.3, we show the application of BDFA to photothermal spectroscopy of methane near 1651 nm. We demonstrate that this technique (as well as fundamentally similar photoacoustic spectroscopy) can greatly benefit from using optical power amplifiers for signal enhancement. Section 4 contains a discussion and conclusions.

2. Materials and Methods (Experimental Setup)

A schematic of the BDFA is shown in Figure 1. A 90 m-long germanosilicate BDF was used as an active fiber (the same fiber was also used in our previous works [21,22]). The GeO_2 content of the fiber was ~50 mol.%. Although its core diameter was only 2.2 μm, it could be spliced to the standard single-mode fiber with relatively low losses (below 1 dB). Bismuth doping combined with the presence of Ge in the fiber core results in luminescence in the spectral region from 1600 to 1800 nm when the fiber is pumped near 1.55 μm [11]. Therefore, the pump source was constructed using a continuous-wave erbium-doped fiber laser (EDFL) amplified with a commercially available erbium/ytterbium-doped fiber amplifier (EYDFA; model GOA-S320 from BKtel, with a maximum output power of 32 dBm). A wavelength division multiplexing (WDM) coupler (from Haphit) was used to couple the pump light into the BDF and out-couple the amplified signals from single-frequency laser diodes: A distributed feed-back (DFB) laser diode was employed at 1651 nm (from NTT Electronics) and a discrete mode (DM) laser diode was applied at 1687 nm (from Eblana Photonics). A polarization-insensitive fiber-based optical isolator (from Opto-link) was placed between the seed source and the BDF to block any backscattered radiation or unabsorbed pump light. It was designed to operate in the C and L band (from 1530 to 1610 nm), but its transmission at longer wavelengths was still relatively high (more than 85% at 1651 nm and ~75% at 1687 nm, including connectors).

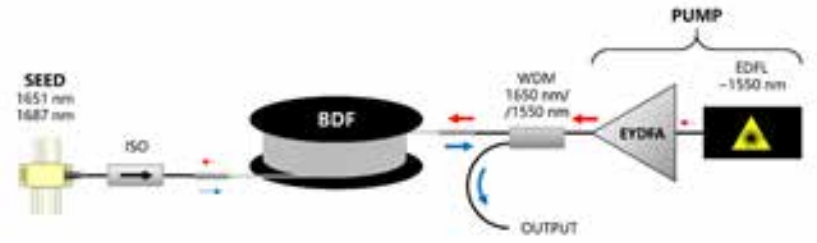

Figure 1. Bismuth-doped fiber amplifier (BDFA) setup: SEED—seed laser diode; ISO—fiber isolator' BDF—bismuth-doped fiber; WDM—wavelength division multiplexing coupler; EYDFA—erbium-ytterbium-doped fiber amplifier; and EDFL—erbium-doped fiber laser (see Section 2.1).

2.1. 1.55 µm Pump Source

As mentioned in the introduction, the main limitation of our previous BDFA configuration was SBS in the bismuth-doped fiber. This phenomenon was affecting the efficiency of BDFA. We believe that, due to backscattering that was observed for high pumping powers, part of the BDF was not pumped sufficiently, so the overall gain was reduced. As a result, the achievable output power was limited. The SBS was observed because a narrowband distributed feed-back (DFB) laser diode (LD) was used as a seed for EYDFA. Therefore, the simplest way to increase the SBS threshold was to use a spectrally broad source which was broader than the gain bandwidth associated with the SBS [23,24].

The schematic diagram of an erbium-doped fiber laser (EDFL) used as a BDFA's pump source is shown in Figure 2. A 10 m-long erbium-doped fiber (EDF; model M5-980-125 from Thorlabs) was pumped using a 974 nm laser diode (from JDSU). A fiber Bragg grating (FBG) was placed inside the ring cavity to make sure that EDFL operated near 1550 nm. The spectrum of the FBG is shown in Figure 3a and the 3 dB bandwidth was ~36 GHz. An optical circulator (from Opto-link) was used not only to insert the FBG into the laser cavity, but also to force a unidirectional operation. An optical coupler (50:50) was used as an output of the laser. Approximately 10 mW of optical power at 1550 nm was obtained with a pump power (at 974 nm) of ~60 mW. Figure 3b shows the optical spectrum emitted from the EDFL with a 3 dB bandwidth of ~4 GHz.

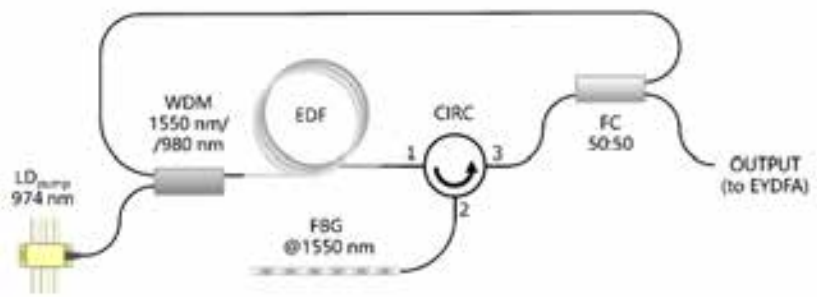

Figure 2. Erbium-doped fiber laser used as a new pump source for BDFA: EDF—erbium-doped fiber; CIRC—optical fiber circulator; FBG—fiber Bragg grating; and FC—fiber coupler.

For comparison, a linewidth of the DFB laser diode used in our previous configurations was also measured. A self-heterodyne method [25] was used, in which light emitted from a narrow-linewidth laser is divided into two beams. One is frequency-shifted by Ω and delayed using an optical fiber (the fiber must be longer than the coherence length of the source under study). This beam is then coupled with the second beam (emitted directly from the source) and the beatnote signal at Ω is analyzed using a radio frequency (RF) spectrum analyzer. Figure 4c shows the RF spectrum recorded using a 1550 nm DFB laser diode as a source and a 600 m-long delay line. Based on this measurement, the linewidth (full width at half maximum) of the pump source used in our previous configurations was estimated to be approximately 1.1 MHz. This is much lower than typical values of the SBS gain

bandwidth [26] and more than three orders of magnitude less than the linewidth of the fiber laser used in this work.

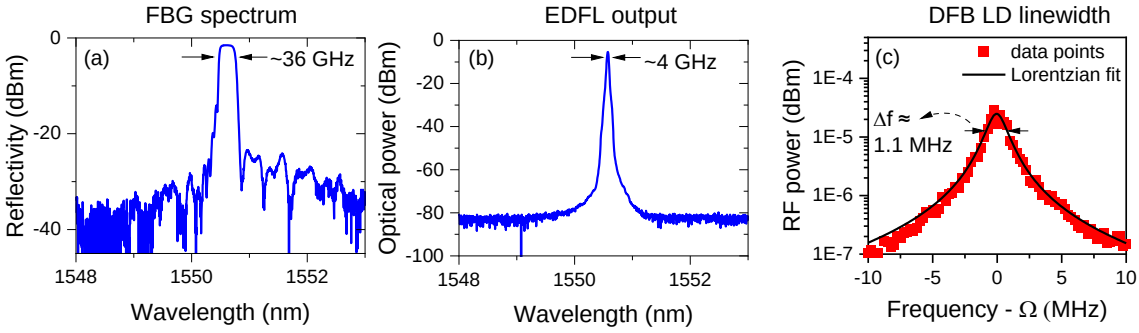

Figure 3. (**a**) Fiber Bragg grating reflectivity near 1550 nm (3 dB bandwidth is ~36 GHz); (**b**) output spectrum of the EDFL emission (3 dB bandwidth of ~4 GHz); (**c**) the result of the self-heterodyne linewidth measurement [25] shows the RF spectrum of the beatnote signal around Ω = 200 MHz. Based on this measurement, the linewidth Δf of the distributed feed-back (DFB) diode was estimated to be ~1.1 MHz.

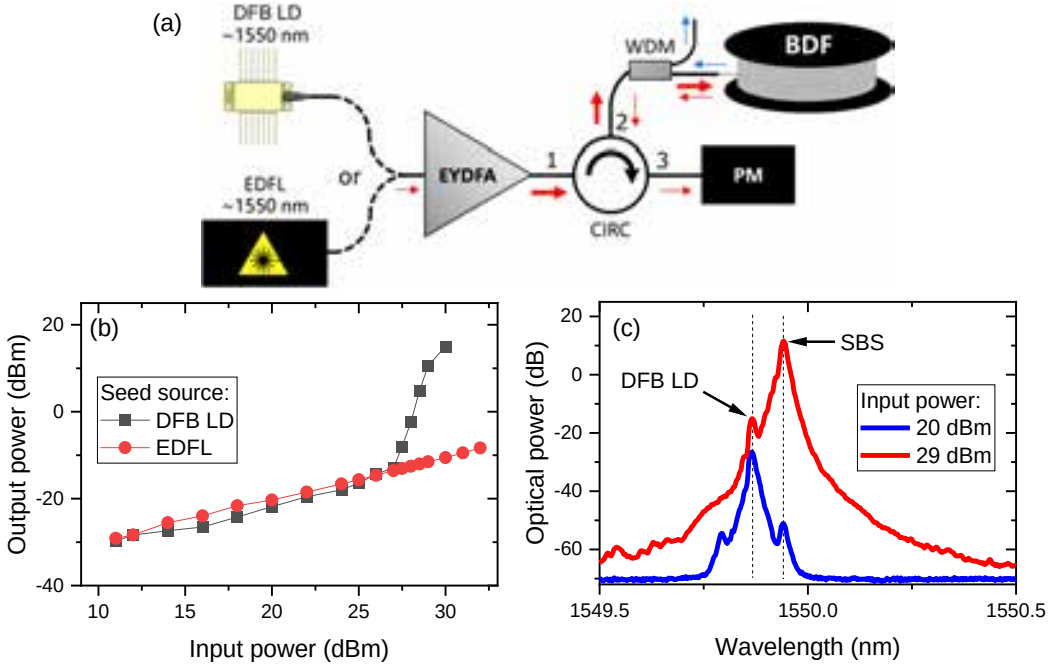

Figure 4. (**a**) Experimental setup used to measure the optical power of light backscattered in the BDF: PM—power meter. A WDM coupler was used to block backscattered amplified spontaneous emission (ASE), as indicated with blue arrows; (**b**) dependence of the backscattered output power on the input power for two light sources; (**c**) spectra of backscattered light recorded with a 0.1 nm resolution for two different input power levels. The peak frequency shifted by ~9.5 GHz that appears for a higher power is clear evidence of stimulated Brillouin scattering (SBS).

3. Results

3.1. SBS Suppression with the New Pump Source

To verify that with the new source, the SBS threshold is reduced, we built the setup shown in Figure 4a. An optical circulator was used to couple the amplified light into a BDF. The third port of the circulator was used to measure the power of the backscattered radiation. Additionally, a WDM coupler

was employed between the circulator and BDF to block backward amplified spontaneous emission (ASE). First, the light from a narrow-linewidth DFB laser diode was used as a seed source for EYDFA. Subsequently, the DFB laser diode was replaced with a new EDFL source. Figure 4b shows how the backscattered optical power depends on the input power (i.e., at the output of the EYDFA) for both seed sources.

In both cases, we observed some linear dependence between the input power and the output (backscattered) power. This might be due to Rayleigh scattering, residual reflection from the splices or connectors, or cross-talk between the 1st and 3rd port of the circulator. However, when a DFB laser diode was used as a seed and the EYDFA power exceeded approximately 27 dBm (~500 mW), SBS became visible. It manifested itself through a rapid, nonlinear increase of the backscattered light power level. This phenomenon was not observed when EDFL was used as a source, even for much higher input powers (up to 32 dBm). The presence of the SBS was additionally confirmed by measuring the spectrum of the backscattered radiation. For a higher input power, a signal frequency shift of ~9.5 GHz was observed, which is expected for Brillouin scattering in a silica fiber doped with Ge [27].

3.2. BDFA Performance

In Figure 5, we present the performance of the BDFA. Figure 5a shows how the output power depends on the pump power for two seed wavelengths: 1651 and 1687 nm. In both cases, an almost linear dependence was obtained for a pump power up to 32 dBm (~1.58 W). The BDFA output power dependence on the seed laser power is shown in Figure 5b. For the highest pump power and the highest available seed power at 1651 nm (15.54 mW), the output power of 163 mW (or 22.1 dBm) was obtained. For a longer wavelength (i.e., 1687 nm), the measured power was even higher: 197 mW (or 22.94 dBm) when a seed power of 5.48 mW was used. These results are almost two times better than those demonstrated previously (87 mW at 1651 nm in [21] and 107 mW at 1687 nm in [22]). The measured gain (shown in Figure 5c) varied from 26 dB (for a low input power at 1687 nm) to approximately 10 dB (for a high input power at 1651 nm).

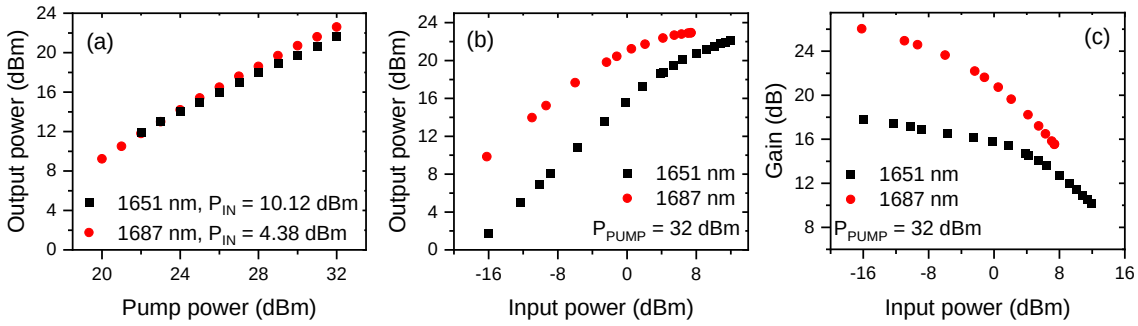

Figure 5. (**a**) BDFA output power versus pump power at 1651 and 1687 nm. (**b**) and (**c**) BDFA output power and gain versus seed power at both wavelengths for a pump power of 32 dBm.

The optical spectra recorded when the BDFA was seeded with a 1651 and 1687 nm laser diode are shown in Figure 6. In both cases, the maximum pump power (32 dBm) was used. A very significant power level difference (more than 40 dB) between the signal and the amplified spontaneous emission (ASE) was obtained. For comparison, the spectra of the two seed sources are also shown in Figure 6a.

Figure 7 presents the stability of the output power of BDFA. It was measured using a power meter (PM100D from Thorlabs with S132C sensor) and a 1651 nm seed laser diode. The input power and the pump power were set to 10.1 and 30 dBm, respectively. The output power was recorded for more than 30 min. The peak-to-peak fluctuations were ~0.32% of the mean value (95.5 mW). Similar output power fluctuations were obtained when lower input powers were used (Figure 7b,c).

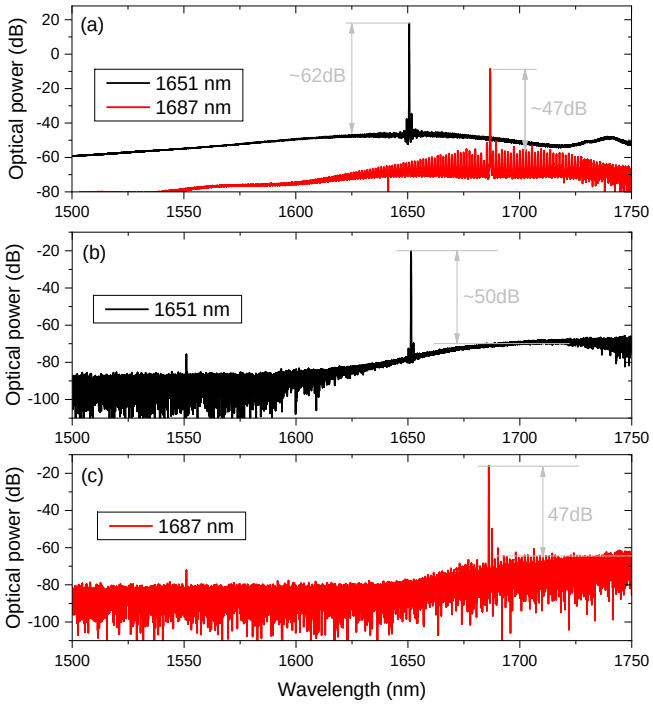

Figure 6. Spectra of the seed sources (**a**) and the output of the amplifier, with a seed wavelength of 1651 (**b**) and 1687 nm (**c**). Pump power was 32 dBm.

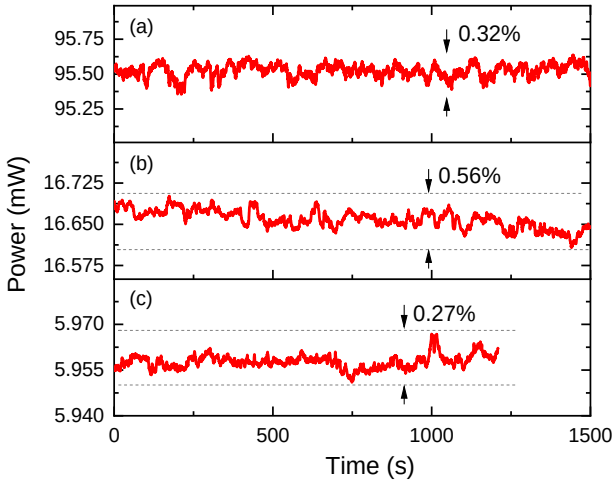

Figure 7. BDFA output powers measured with a 1651 nm seed and 30 dBm pump power. The input powers were ~10 (**a**), ~0.5 (**b**), and ~0.2 mW (**c**). All data were acquired after warm-up (~1 h).

3.3. Photothermal Spectroscopy Using a BDFA-Amplified Source

In order to demonstrate how BDFA can be used in laser spectroscopy, a setup that enables photothermal spectroscopy (PTS) to be performed was built. PTS can be used to detect and quantify gas samples by observing indirect effects of light–matter interaction. Energy absorbed by gas is turned to heat, leading to a local rise of the gas temperature and change of the gas refractive index. The refractive index change can be measured using, e.g., an interferometric setup [28,29]. Because the photothermal signal is proportional to the absorbed energy, an optical amplifier can be used to improve the performance of PTS. This was previously demonstrated using photoacoustic spectroscopy (a technique which is fundamentally similar to PTS) performed in a more convenient telecom wavelength region (below 1.6 μm, where erbium-doped fiber amplifiers can be used) [30–34]. Here, we show BDFA-enhanced PTS of methane using the setup schematically shown in Figure 8.

The light emitted from a 1651 nm DFB laser diode was amplified with the BDFA and entered the gas sample (enclosed in a glass cell) through a 90:10 fiber coupler. The DFB laser diode was current modulated with a sinewave (f_m = 0.5 kHz) to produce periodic changes of the refractive index inside the gas cell. These changes were measured using an interferometer formed between two fiber couplers (90:10 and 50:50). Additional saw-tooth modulation (1 Hz) was added to provide a wavelength scan across the target transition. The light from the 1550 nm DFB laser diode was used as a probe beam. An acousto-optic frequency shifter/modulator (AOM) driven at f_a = 200 MHz was placed in one arm of the interferometer, enabling heterodyne detection of the photothermal signal: Changes of the optical length in one arm were detected as changes of the phase of the heterodyne signal. The main advantage of heterodyne-based detection [35] compared to homodyne-based sensing is that a heterodyne-based setup does not require the arms of the interferometer to be stabilized [36,37]. A high-speed lock-in amplifier (UHFLI from Zurich Instruments) was used to perform phase demodulation of the beat note at 200 MHz, as well as subsequent signal demodulation (filtering) at $2 \times f_m$ (this helps with removing background signals due to, e.g., non-resonant absorption in the setup).

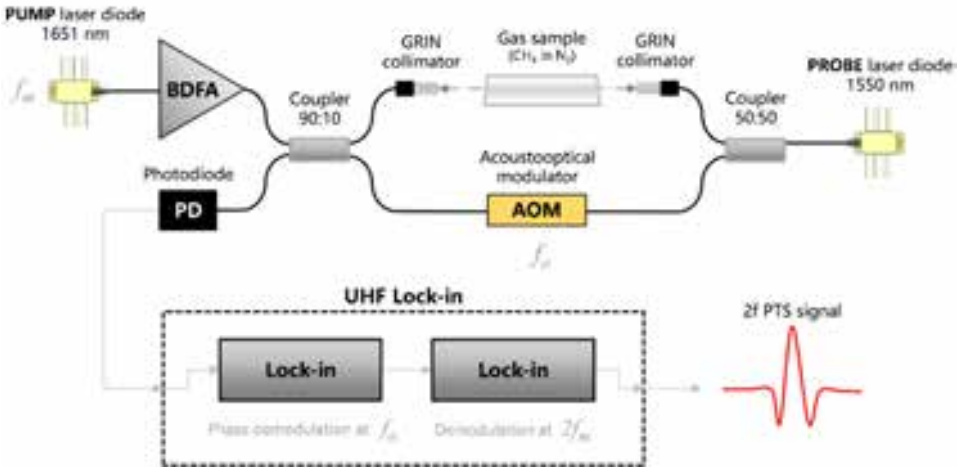

Figure 8. Heterodyne interferometric setup for photothermal gas detection.

Figure 9a shows the PTS spectra measured for a 100 mm-long sample containing 4.29% methane (balanced with nitrogen, total pressure of 740 torr; the concentrations was determined based on direct absorption measurement and spectral fitting with data from the HITRAN database [38]). Four different powers at the output of BDFA were used (the optical power was measured after the collimator and before the gas cell). 2*f* PTS spectra are baseline-free and their amplitude clearly depends on the optical power.

A linear dependence between the signal to noise ratio (SNR) and the optical power level was also confirmed, as shown in Figure 9b. For this measurement, a shorter gas cell (25 mm) was used (with a methane concentration of approximately 5.35%). The signal was measured as the 2*f* PTS amplitude at the transition center and the noise was calculated as the standard deviation of the signal recorded when the sample was removed from the setup. Based on this measurement (i.e., SNR ≈ 52 for the incident power of ~120 mW), we could calculate the noise equivalent concentration, which was shown to be approximately 19.3 ppm × m × $Hz^{-1/2}$, corresponding to the noise equivalent absorbance of ~7.2×10^{-4} $Hz^{-1/2}$. This result is comparable to the sensitivity demonstrated previously with a similar method [35]. We expect that a significantly better detection limit could be obtained if photothermal spectroscopy was performed inside a hollow core fiber [36,37].

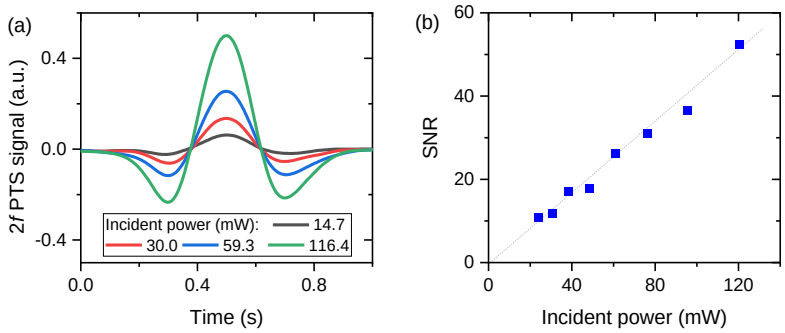

Figure 9. (**a**) 2*f* photothermal spectroscopy (PTS) signals for various incident power levels for a 100 mm-long cell with a methane concentration of 4.29%. A 1 Hz saw-tooth modulation was used to scan the wavelength across the methane transition near 1651 nm. (**b**) The dependence of the 2*f* PTS signal/noise ratio on the incident power at 1651 nm; the signal was measured using a 25 mm-long cell with a methane concentration of 5.35%.

4. Discussion

In this paper, the bismuth-doped fiber amplifier was presented. The new fiber-based pump source helped to suppress the unwanted SBS (observed in the previous setup) and enabled the delivery of a much higher pumping power (up to almost 1.6 W) to the BDF compared to the configuration presented in [21,22]. The performance of the amplifier was analyzed at two wavelengths: 1651 and 1687 nm. The output powers of 163 mW (1651 nm) and 197 mW (1687 nm) were obtained. These power levels are almost two times higher than those demonstrated earlier with the previous BDFA configuration [21,22]. More importantly, the linear dependence between the output power and the pump power suggests that a further increase of the output power should be possible when a higher pump power level is used.

In addition to the high power at the output, the BDFA presented in this paper also offers a significant small signal gain: 18 dB at 1651 nm and 26 dB at 1687 nm. These values are higher than previously published for BDFAs [17] and also higher then reported for the short-wavelength Al/Tm-doped fiber amplifier presented in [7]. A similar small signal gain was obtained in [8], where a Ge/Tm-doped fiber was used.

A comparison of the presented BDFA with some previously demonstrated amplifiers is presented in Table 1. The BDFA reported in this work uses a longer fiber than Tm-doped fiber amplifiers, but provides a higher output power while requiring a smaller pump power.

Table 1. Summary of the parameters of various previously reported fiber amplifiers operating near 1650 nm and the results obtained in this work.

Ref.	Fiber Type	Fiber Length	Pump Power	Small Signal Gain @1650 nm	Output Power @1650 nm
[7]	Al/Tm-doped	5 m	37 dBm	8 dB	8 dBm
[8]	Ge/Tm-doped	4.5 m	36.9 dBm	18.7 dB	15 dBm
[17]	Ge/Bi-doped	50 m	24.77 dBm	~5 dB	10 dBm (@1680 nm)
This work	Ge/Bi-doped	90 m	32 dBm	18 dB	22.1 dBm

We also analyzed the noise at the output of the amplifier. Output power fluctuations below 1% were obtained not only for high, but also for low, input powers. These features (high gain and output power stability for low input powers) make the presented BDFA an attractive booster amplifier in the wavelength region that cannot be easily covered by semiconductor amplifiers.

As a potential application of BDFA, we have presented the photothermal spectroscopy of methane at 1651 nm. We have demonstrated that the amplifier can be used to improve the signal amplitude and

signal/noise ratio. Similar sensitivity enhancement can be expected when more common photoacoustic spectroscopy is used [39,40].

Author Contributions: Bismuth-doped fiber design, fabrication, and characterization: A.M.K., S.V.A., A.S.L., and S.V.F.; BDFA design and characterization: G.G., M.K. (Małgorzata Kaleta), and M.N.; Photothermal spectroscopy experiments: M.K. (Monika Krajewska), G.G., and M.N.; manuscript writing: M.N., G.G., and S.V.F. All authors have read and agreed to the published version of the manuscript.

Funding: This research was funded by The National Science Centre, Poland, grant no. UMO-2018/29/B/ST7/01730. M.N. acknowledges funding within the National Laboratory for Photonics and Quantum Technologies (NLPQT) project (POIR.04.02.00-00-B003/18), co-financed by the European Regional Development Fund (ERDF), and the Russian Science Foundation, grant no. 19-72-10003 (fabrication and characterization of Bi-doped fiber).

Conflicts of Interest: The authors declare no conflict of interest.

References

1. Crotti, C.; Deloison, F.; Alahyane, F.; Aptel, F.; Kowalczuk, L.; Legeais, J.-M.; Peyrot, D.A.; Savoldelli, M.; Plamann, K. Wavelength optimization in femtosecond laser corneal surgery. *Investig. Ophthalmol. Vis. Sci.* **2013**, *54*, 3340–3349. [CrossRef]
2. Qin, Y.; Batjargal, O.; Cromey, B.; Kieu, K. All-fiber high-power 1700 nm femtosecond laser based on optical parametric chirped-pulse amplification. *Opt. Express* **2020**, *28*, 2317–2325. [CrossRef]
3. Zhang, E.J.; Teng, C.C.; van Kessel, T.G.; Klein, L.; Muralidhar, R.; Wysocki, G.; Green, W.M.J. Field deployment of a portable optical spectrometer for methane fugitive emissions monitoring on oil and gas well pads. *Sensors* **2019**, *19*, 2707. [CrossRef]
4. Tian, X.; Cao, Y.; Chen, J.; Liu, K.; Wang, G.; Tan, T.; Mei, J.; Chen, W.; Gao, X. Dual-gas sensor of CH4/C2H6 based on wavelength modulation spectroscopy coupled to a home-made compact dense-pattern multipass cell. *Sensors* **2019**, *19*, 820. [CrossRef]
5. Liu, K.; Wang, L.; Tan, T.; Wang, G.; Zhang, W.; Chen, W.; Gao, X. Highly sensitive detection of methane by near-infrared laser absorption spectroscopy using a compact dense-pattern multipass cell. *Sens. Actuators B Chem.* **2015**, *220*, 1000–1005. [CrossRef]
6. Cheng, G.; Cao, Y.; Liu, K.; Zhu, G.; Wang, G.; Gao, X. Photoacoustic measurement of ethane with near-infrared DFB diode laser. *J. Spectrosc.* **2018**, *2018*, 9765806. [CrossRef]
7. Li, Z.; Jung, Y.; Daniel, J.M.O.; Simakov, N.; Tokurakawa, M.; Shardlow, P.C.; Jain, D.; Sahu, J.K.; Heidt, A.M.; Clarkson, W.A.; et al. Exploiting the short wavelength gain of silica-based thulium-doped fiber amplifiers. *Opt. Lett.* **2016**, *41*, 2197–2200. [CrossRef]
8. Chen, S.; Jung, Y.; Alam, S.; Richardson, D.J.; Sidharthan, R.; Ho, D.; Yoo, S.; Daniel, J.M.O. Ultra-short wavelength operation of thulium-doped fiber amplifiers and lasers. *Opt. Express* **2019**, *27*, 36699–36707. [CrossRef]
9. Tsuzaki, T.; Kakui, M.; Hirano, M.; Onishi, M.; Nakai, Y.; Nishimura, M. Broadband discrete fiber Raman amplifier with high differential gain operating over 1.65 μm-band. In Proceedings of the OFC 2001 Optical Fiber Communication Conference and Exhibit. Technical Digest Postconference Edition (IEEE Cat. 01CH37171), Anaheim, CA, USA, 17 March 2001; Volume 1, p. MA3.
10. Bauer, R.; Legg, T.; Mitchell, D.; Flockhart, G.M.H.; Stewart, G.; Johnstone, W.; Lengden, M. Miniaturized photoacoustic trace gas sensing using a raman fiber amplifier. *J. Light. Technol.* **2015**, *33*, 3773–3780. [CrossRef]
11. Dianov, E.M. Bismuth-doped optical fibers: A challenging active medium for near-IR lasers and optical amplifiers. *Light Sci. Appl.* **2012**, *1*, e12. [CrossRef]
12. Thipparapu, N.K.; Wang, Y.; Wang, S.; Umnikov, A.A.; Barua, P.; Sahu, J.K. Bi-doped fiber amplifiers and lasers. *Opt. Mater. Express* **2019**, *9*, 2446–2465. [CrossRef]
13. Bufetov, I.A.; Melkumov, M.A.; Firstov, S.V.; Riumkin, K.E.; Shubin, A.V.; Khopin, V.F.; Guryanov, A.N.; Dianov, E.M. Bi-doped optical fibers and fiber lasers. *IEEE J. Sel. Top. Quantum Electron.* **2014**, *20*, 111–125. [CrossRef]
14. Thipparapu, N.K.; Wang, Y.; Umnikov, A.A.; Barua, P.; Richardson, D.J.; Sahu, J.K. 40 dB gain all fiber bismuth-doped amplifier operating in the O-band. *Opt. Lett.* **2019**, *44*, 2248. [CrossRef] [PubMed]
15. Thipparapu, N.K.; Umnikov, A.A.; Barua, P.; Sahu, J.K. Bi-doped fiber amplifier with a flat gain of 25 dB operating in the wavelength band 1320–1360 nm. *Opt. Lett.* **2016**, *41*, 1518–1521. [CrossRef]

16. Dianov, E.M.; Mel'kumov, M.A.; Shubin, A.V.; Firstov, S.V.; Khopin, V.F.; Gur'yanov, A.N.; Bufetov, I.A. Bismuth-doped fibre amplifier for the range 1300–1340 nm. *Quantum Electron.* **2009**, *39*, 1099–1101. [CrossRef]
17. Firstov, S.V.; Alyshev, S.V.; Riumkin, K.E.; Khopin, V.F.; Guryanov, A.N.; Melkumov, M.A.; Dianov, E.M. A 23-dB bismuth-doped optical fiber amplifier for a 1700-nm band. *Sci. Rep.* **2016**, *6*, 28939. [CrossRef]
18. Kharakhordin, A.V.; Alyshev, S.V.; Firstova, E.G.; Lobanov, A.S.; Khopin, V.F.; Khegai, A.M.; Melkumov, M.A.; Guryanov, A.N.; Firstov, S.V. Lasing properties of thermally treated GeO2-SiO2 glass fibers doped with bismuth. *Appl. Phys. B* **2020**, *126*, 87. [CrossRef]
19. Alyshev, S.; Kharakhordin, A.; Firstova, E.; Khegai, A.; Melkumov, M.; Khopin, V.; Lobanov, A.; Guryanov, A.; Firstov, S. Photostability of laser-active centers in bismuth-doped GeO2-SiO2 glass fibers under pumping at 1550 nm. *Opt. Express* **2019**, *27*, 31542–31552. [CrossRef]
20. Firstov, S.V.; Alyshev, S.V.; Riumkin, K.E.; Khegai, A.M.; Kharakhordin, A.V.; Melkumov, M.A.; Dianov, E.M. Laser-active fibers doped with bismuth for a wavelength region of 1.6–1.8 µm. *IEEE J. Sel. Top. Quantum Electron.* **2018**, *24*, 1–15. [CrossRef]
21. Nikodem, M.; Khegai, A.; Firstov, S.V. Single-frequency bismuth-doped fiber power amplifier at 1651 nm. *Laser Phys. Lett.* **2019**, *16*, 115102. [CrossRef]
22. Gomolka, G.; Khegai, A.M.; Alyshev, S.V.; Lobanov, A.S.; Firstov, S.V.; Nikodem, M. Characterization of a single-frequency bismuth-doped fiber power amplifier with a continuous wave and modulated seed source at 1687 nm. *Appl. Opt.* **2020**, *59*, 1558–1563. [CrossRef] [PubMed]
23. Zeringue, C.; Dajani, I.; Naderi, S.; Moore, G.T.; Robin, C. A theoretical study of transient stimulated Brillouin scattering in optical fibers seeded with phase-modulated light. *Opt. Express* **2012**, *20*, 21196–21213. [CrossRef] [PubMed]
24. Garmire, E. Stimulated brillouin review: Invented 50 years ago and applied today. *Int. J. Opt.* **2018**, *2018*, 2459501. [CrossRef]
25. Okoshi, T.; Kikuchi, K.; Nakayama, A. Novel method for high resolution measurement of laser output spectrum. *Electron. Lett.* **1980**, *16*, 630–631. [CrossRef]
26. Preussler, S.; Schneider, T. Stimulated brillouin scattering gain bandwidth reduction and applications in microwave photonics and optical signal processing. *Opt. Eng.* **2015**, *55*, 1–11. [CrossRef]
27. Yeniay, A.; Delavaux, J.-M.; Toulouse, J. Spontaneous and stimulated brillouin scattering gain spectra in optical fibers. *J. Light. Technol.* **2002**, *20*, 1425. [CrossRef]
28. Owens, M.A.; Davis, C.C.; Dickerson, R.R. A photothermal interferometer for gas-phase ammonia detection. *Anal. Chem.* **1999**, *71*, 1391–1399. [CrossRef] [PubMed]
29. Waclawek, J.P.; Kristament, C.; Moser, H.; Lendl, B. Balanced-detection interferometric cavity-assisted photothermal spectroscopy. *Opt. Express* **2019**, *27*, 12183–12195. [CrossRef]
30. Webber, M.E.; Pushkarsky, M.; Patel, C.K.N. Fiber-amplifier-enhanced photoacoustic spectroscopy with near-infrared tunable diode lasers. *Appl. Opt.* **2003**, *42*, 2119–2126. [CrossRef]
31. He, Y.; Ma, Y.; Tong, Y.; Yu, X.; Tittel, F.K. HCN ppt-level detection based on a QEPAS sensor with amplified laser and a miniaturized 3D-printed photoacoustic detection channel. *Opt. Express* **2018**, *26*, 9666–9675. [CrossRef]
32. Wu, H.; Sampaolo, A.; Dong, L.; Patimisco, P.; Liu, X.; Zheng, H.; Yin, X.; Ma, W.; Zhang, L.; Yin, W.; et al. Quartz enhanced photoacoustic H_2S gas sensor based on a fiber-amplifier source and a custom tuning fork with large prong spacing. *Appl. Phys. Lett.* **2015**, *107*, 111104. [CrossRef]
33. Wu, H.; Dong, L.; Liu, X.; Zheng, H.; Yin, X.; Ma, W.; Zhang, L.; Yin, W.; Jia, S. Fiber-amplifier-enhanced QEPAS sensor for simultaneous trace gas detection of NH3 and H2S. *Sensors* **2015**, *15*, 26743–26755. [CrossRef]
34. Ma, Y.; He, Y.; Tong, Y.; Yu, X.; Tittel, F.K. Ppb-level detection of ammonia based on QEPAS using a power amplified laser and a low resonance frequency quartz tuning fork. *Opt. Express* **2017**, *25*, 29356–29364. [CrossRef]
35. Krzempek, K.; Dudzik, G.; Abramski, K.; Wysocki, G.; Jaworski, P.; Nikodem, M. Heterodyne interferometric signal retrieval in photoacoustic spectroscopy. *Opt. Express* **2018**, *26*, 1125–1132. [CrossRef]
36. Jin, W.; Cao, Y.; Yang, F.; Ho, H.L. Ultra-sensitive all-fibre photothermal spectroscopy with large dynamic range. *Nat. Commun.* **2015**, *6*, 6767. [CrossRef]
37. Yao, C.; Wang, Q.; Lin, Y.; Jin, W.; Xiao, L.; Gao, S.; Wang, Y.; Wang, P.; Ren, W. Photothermal CO detection in a hollow-core negative curvature fiber. *Opt. Lett.* **2019**, *44*, 4048–4051. [CrossRef]

38. Rothman, L.S.; Gordon, I.E.; Barbe, A.; Benner, D.C.; Bernath, P.F.; Birk, M.; Boudon, V.; Brown, L.R.; Campargue, A.; Champion, J.-P.; et al. The HITRAN 2008 molecular spectroscopic database. *J. Quant. Spectrosc. Radiat. Transf.* **2009**, *110*, 533–572. [CrossRef]
39. Hu, L.; Zheng, C.; Zhang, M.; Yao, D.; Zheng, J.; Zhang, Y.; Wang, Y.; Tittel, F.K. Quartz-enhanced photoacoustic spectroscopic methane sensor system using a quartz tuning fork-embedded, double-pass and off-beam configuration. *Photoacoustics* **2020**, *18*, 100174. [CrossRef]
40. Milde, T.; Hoppe, M.; Tatenguem, H.; Assmann, C.; Schade, W.; Sacher, J. Comparison of the spectral excitation behavior of methane according to InP, GaSb, IC, and QC lasers as excitation source by sensor applications. *Appl. Opt.* **2019**, *58*, C84–C91. [CrossRef]